Optimal Control of a Laser Source to Generate a Minimum Time Trajectory of a Droplet in a Liquid Layer

Francesco Biral*, Enrico Bertolazzi*, Paolo Bosetti*, Alberto De Marchi* and Martin M. Hanczyc†
*Department of Industrial Engineering
University of Trento
Trento, Italy I-38123
Email: paolo.bosetti@unitn.it
†Centre for Integrative Biology
University of Trento
Trento, Italy I-38123
Email: martin.hanczyc@unitn.it

***Abstract*—This paper describes the use of optimal control theory applied to the motion of a low-power laser beam to precisely move a droplet in a liquid layer by means of the force on the liquid-liquid interface arising due to the surrounding thermal field (thermocapillary force and Marangoni effect). The form of heat field equations is approximated by the solution of a finite sum of laser pulses, whose analytical solution can be explicitly derived. In this way, the model of the system does not contain any partial differential equation (PDE). Optimization is performed by using the direct approach method and the *fmincon* solver provided by Matlab. The initial guess is found with a simple model predictive controller. Perspective applications of this technology include beam-controlled targeting of pharmaceuticals in organic tissues.**

***Keywords*—Optimal control; model predictive control; droplet; thermocapillary force; targeting of pharmaceuticals**

I. Introduction

The manipulation of liquid droplets suspended in another liquid can be achieved through thermocapillary motion through a nonuniform heat distribution in the system [1]. This nonuniformity results in thermocapillary stresses near the droplet interface with liquid flowing from the hot (lower surface tension) to cold side (higher surface tension) through Marangoni flows. In systems where viscosity dominates, the droplet will migrate. This resulting fluid flow dynamics allows for the movement of the droplet directionally through the system (e.g. for bubbles see [2]; for liquid droplets see [3]; for liquid droplets of spherical and aspherical shape see [4] and [5]).

The manipulation of droplets through heat gradient induced Marangoni flows have found practical applications in microfluidics including controlled mixing, confining, filtering, trapping and pumping of droplets [6]. The application of light energy to induce quick and controlled thermal gradients has also been explored [7], [8], [9]. By using optothermal capillary control, multidroplet manipulation and fusion has been demonstrated [10] as well as high speed droplet sorting [11].

The Authors have been exploring the dynamical motion of liquid droplets in a second immiscible liquid phase [12]. These droplets either have on board chemical potential which then induces and fuels a Marangoni flow system for autonomous motion [13], or the droplets are more passive and only respond to local chemical gradients in the system. Even in the simpler passive system the dynamical fluid motion of droplets allows for the completion of simple tasks such as solving mazes [14].

Interfacing dynamic droplets with electromechanical control can allow for the precise manipulation of droplets [10], [11], the sustenance of non-equilibrium states [15], and the exploration of the dynamical phase spaces [16].

In the present work, the Authors develop the use of optimal control theory applied to the motion of a low-power laser beam to precisely move a droplet through thermocapillary action. This methodology has application in the broader context of fluid mixing, tuning of interfacial properties and combinatorial processes including reactive combinatorial chemistry when droplets are precisely positioned to fuse. This will allow the control of sensitive chemical reactions on demand under controlled laboratory conditions as applied to biochemical analyses and material synthesis.

Currently this technology will add a fundamental control layer to our current EU project EVOBLISS that uses a robotic platform for the manipulation of chemical droplets [17]. In order to provide effective functionality for the project the optimal control mechanism will be implemented in real time to interface with the dynamics of the chemical droplets [15]. This is a novel substantiation of such an approach and the real time component is critical for precise manipulation of far from equilibrium chemical systems. This type of platform and control mechanism is distinct from often used microfluidics where microsized droplets are produced and manipulated almost exclusively through the imposed architectures of the microfluidic device [18], [19]. Instead here it is of interest to take advantage of targeted control mechanisms to temporarily interface with the dynamic droplets but then once the control is achieved release the droplets to allow them perform tasks more autonomously. It is hoped that in the future the precise positional control of reactive chemistries can be effected in complex environments such as organ tissues to deliver and

978-1-5090-4171-8/16/$31.00

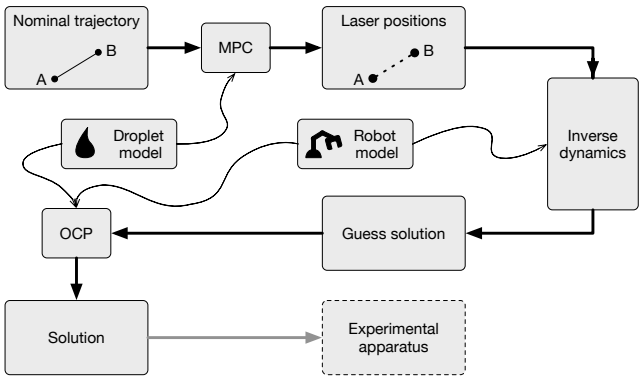

Fig. 1. Schematics of control method

perhaps trigger the synthesis and release of therapeutics on site.

II. Modeling

The work here presented is based on the idea of moving a droplet in its fluid environment by "pushing" it with the thermal gradient that results from heating the surrounding liquid with a laser beam. It is as letting the droplet surfing on the wave produced by a localized heat source.

In order to control the motion of the droplet by moving the laser spot about its proximity, the *trajectory* (i.e. the path and its time-history) of the laser spot itself has to be calculated according to the dynamics of the droplet and of the thermal field itself, so that the resulting laser motion is neither too fast—so that the droplet would loose tracking—nor too slow—which would result in the laser beam hitting the droplet itself.

Consequently, it is needed a set of analytical models (perhaps approximated) of the droplet and of the system actuating the laser position—which will be referred to as the *robot* in the followings.

These models are then used for calculating the optimum time-sequence of *controls* that ensure the robot moves the laser at the optimal speed (neither too fast nor too slow) and along the desired trajectory in its liquid medium.

The schematics in Fig. 1 summarizes the approach: the whole process starts from the initial definition of the desired, nominal trajectory. With the approach known as *Model Predictive Control* (MPC), the model of the droplet dynamics is then used for calculating the time-sequence of laser spot positions that would drive the droplet from its initial position to the target one. This sequence of position is then converted in a sequence of robot *controls* (or inputs to the robot motors) thanks to the robot model and to its inverse dynamics. The result of this step is the *guess solution*, i.e. a tentative, approximate solution that still does not ensure an optimal performance, and which is eventually used for solving the *Optimal Control Problem* (OCP). The latter, finally, produces an optimal time sequence of controls that allows to drive the droplet from A to B maximizing the performance and yet complying with a given set of constraints.

The following sections are detailedly describing the models of the dynamics for droplet and robot, and the numerical approaches taken for solving the two-step optimization approach (MPC + OCP).

A. Model of Laser Heating

For a source of intensity I_0, the transmitted intensity I of an electromagnetic wave penetrating a material is given by Beer's law

$$I(z) = I_0 e^{-\beta(\lambda)z} \tag{1}$$

where $\beta(\lambda)$ is the absorption coefficient that depends on laser wavelength λ and z is the path length. Let us focus on an absorbing layer of thickness Δz along the beam propagation direction. For a weakly absorbing medium, i.e. $\beta(\lambda)\Delta z \ll 1$, the intensity $I(z)$ can be approximated as a first-order term

$$I(z) \approx I_0 \left[1 - \beta(\lambda)z\right] \tag{2}$$

Therefore the intensity reduction per unit thickness is $\beta(\lambda)I_0$. Assuming that all the light energy absorbed by the medium is converted instantly to heat, the intensity reduction per unit thickness is the thermal energy deposited in the medium per unit volume per unit time

$$\dot{q} = \beta(\lambda)I_0 \tag{3}$$

Let us define temperature field w, laser position $\mathbf{x}_L$ and power p_L, heat sink temperature $\bar{w}$ and the spatial domain $\Omega \subset \mathbb{R}^2$ with boundary $\partial\Omega$, time-space domain $\tilde{\Omega} = (t_i, t_f) \times \Omega$ with spatial boundary $\partial\tilde{\Omega} = (t_i, t_f) \times \tilde{\Omega}$. Transient thermal dynamics is governed by the unsteady heat equation assuming constant liquid properties (specific mass ρ, specific heat c_p, thermal conductivity k, thermal diffusivity $\alpha = k/\rho c_p$) and absence of any mass transport. For $(t, \mathbf{x}) \in \tilde{\Omega}$ it reads

$$\rho c_p \frac{\partial w}{\partial t}(t, \mathbf{x}) = k\nabla^2 w(t, \mathbf{x}) + \dot{q}(t, \mathbf{x}) \tag{4}$$

For the sake of simplicity, constant homogeneous Dirichlet boundary conditions, i.e. $\bar{w}(t, \mathbf{x}) = 0 \ \forall (t, \mathbf{x}) \in \partial\tilde{\Omega}$, are selected. Moreover, laser-induced incident intensity is assumed to be Gaussian with characteristic radius r_L and with fixed wavelength, so that absorption coefficient $\beta = \beta(\lambda)$ is constant.

$$\dot{q}(t, \mathbf{x}) = \frac{2\beta}{\pi r_L^2} \, p_L \, e^{-2\frac{\|\mathbf{x}-\mathbf{x}_L\|^2}{r_L^2}} \tag{5}$$

So the governing equation expressed in polar coordinates (centred in laser pulse position) reads

$$\rho c_p \frac{\partial w}{\partial t}(t, \mathbf{x}) = k\nabla^2 w(t, \mathbf{x}) + \frac{2\beta p_L}{\pi r_L^2} \, e^{-2\frac{r(\mathbf{x})^2}{r_L^2}} \, \delta(t - t_i) \tag{6}$$

Let us recall the solution $\tilde{w}$ for an instantaneous point-wise heat release (energy $p_L \Delta t$ in $r = 0$ at time $t = 0$) and build by similarity a function θ with free parameters a, b and c

$$\begin{aligned} \tilde{w} &= \bar{w} + \frac{\beta p_L \Delta t}{\pi \rho c_p} \frac{1}{4\alpha t} e^{-r^2/(4\alpha t)} \\ \theta &= \bar{w} + \frac{a}{ct + 1} e^{-br^2/(ct+1)} \end{aligned} \tag{7}$$

Considering the function θ, it shall be assessed if it could be a solution of the heat equation above, and in that case its coefficients will be matched. Substituting θ and its derivatives into the heat equation, after some calculations, one gets two conditions on coefficients:

$$c = 4\alpha b \qquad b = \frac{2}{r_L^2}, \tag{8}$$

where $\alpha = k/(\rho c_p)$ is the liquid thermal diffusivity. Then, by the energy conservation law, one can also write:

$$\begin{aligned} \beta p_L \Delta t &= \int_\Omega \rho c_p \left(\theta - \bar{w}\right) d\Omega \\ &= \int_0^{2\pi} \int_0^{\infty} \rho c_p \frac{a}{ct+1} e^{-br^2/(ct+1)} r dr d\theta \\ &= \pi \rho c_p \frac{a}{b} \\ &\Downarrow \\ a &= \frac{\beta p_L \Delta t}{\pi \rho c_p} b \end{aligned} \tag{9}$$

Thus, by solving for coefficients a, b and c and substituting into function θ, one find the analytical expression of temperature field due to an instantaneous Gaussian laser pulse. Notice that for every finite r_L the solution satisfies:

$$\begin{aligned} \lim_{r\to\infty} \theta &= \bar{w} \\ \lim_{t\to\infty} \theta &= \bar{w} \end{aligned} \tag{10}$$

For $t > 0$, it results:

$$w(t, \mathbf{x}) = \bar{w} + \frac{2}{\pi} \frac{\beta p_L \Delta t}{\rho c_p} \frac{1}{8\alpha t + r_L^2} e^{-2\frac{r(\mathbf{x})^2}{8\alpha t + r_L^2}} \tag{11}$$

where $r(\mathbf{x})$ is the distance between $\mathbf{x}$ and heat release position $\mathbf{x}_L$.

Then, the exact thermal field generated by a laser beam trajectory $\mathbf{x}_L(t)$ and laser power profile $p_L(t)$ can be computed by the convolution integral (thanks to linearity), for $t > 0$. Actually it turns out that this integral is quite involved, so it is preferable to build an equispaced time grid and approximate the convolution integral as the finite sum of instantaneous laser pulses.

$$\begin{aligned} w(t, \mathbf{x}) &= \bar{w} + \frac{2}{\pi} \frac{\beta}{\rho c_p} \int_0^t \frac{p_L(\tau)}{8\alpha(t-\tau) + r_L^2} e^{-2\frac{\|\mathbf{x} - \mathbf{x}_L(\tau)\|^2}{8\alpha(t-\tau) + r_L^2}} d\tau \\ &\Downarrow \\ w(t_k, \mathbf{x}) &\approx \bar{w} + \frac{2}{\pi} \frac{\beta \Delta t}{\rho c_p} \sum_{j=0}^{k} \frac{p_{L,j}}{8\alpha(k-j)\Delta t + r_L^2} e^{-2\frac{\|\mathbf{x} - \mathbf{x}_{L,j}\|^2}{8\alpha(k-j)\Delta t + r_L^2}} \end{aligned} \tag{12}$$

One can than compute explicitly the thermal gradient, considering a cylindrical system of coordinates for each laser pulse and projecting then in the absolute Cartesian system:

$$\begin{aligned} &\nabla w(t_k, \mathbf{x}) = \\ &= -\frac{8}{\pi} \frac{\beta \Delta t}{\rho c_p} \sum_{j=0}^{k} \frac{p_{L,j}(\mathbf{x} - \mathbf{x}_{L,j})}{\left[8\alpha(k-j)\Delta t + r_L^2\right]^2} e^{-2\frac{\|\mathbf{x} - \mathbf{x}_{L,j}\|^2}{8\alpha(k-j)\Delta t + r_L^2}} \end{aligned} \tag{13}$$

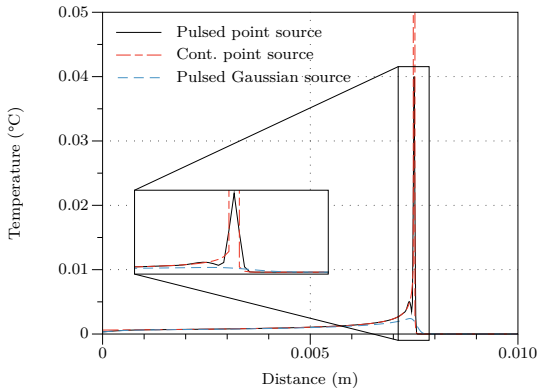

Fig. 2. Temperature field induced by laser heating: finite sum approximation with time step $\Delta t = 10\,\mathrm{ms}$ (spatial resolution $20\,\mu\mathrm{m}$)

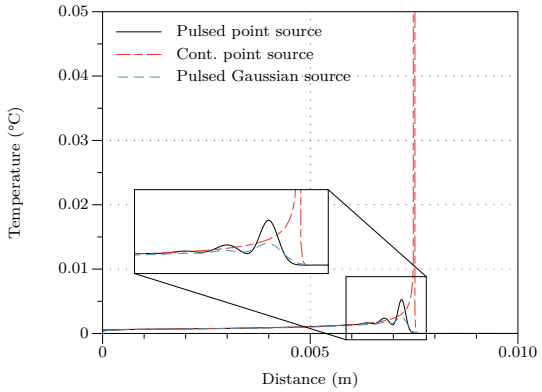

Fig. 3. Temperature field induced by laser heating: finite sum approximation with time step $\Delta t = 40\,\mathrm{ms}$ (spatial resolution $20\,\mu\mathrm{m}$)

The approximation of temperature field using a finite sum of pulses depends on the time step Δt, that is the time interval between two consecutive laser pulses. In order to validate this approach and to estimate an upper bound for the time step, it is useful to compare the result with an analytical solution. Temperature profile induced by a continuous—not pulsed—point heat source moving at constant speed is known in literature. Approximations of this analytical solution with finite sum of pulses are shown in Fig. 2 and Fig. 3, considering two different time steps. Moreover, temperature field approximation in case of Gaussian laser beam is reported. Parameters are characteristic radius $r_L = 0.2\,\mathrm{mm}$, constant speed $10\,\mathrm{mm/s}$, power laser and liquid properties from I. It is evident that analytical and *finite-sum* profiles converge as time step diminishes. As expected, in the neighbourhood of laser spot, predicted temperature due to point or Gaussian source is quite different, being in the latter case much smoother. Thanks to this, the sensitivity of temperature approximation in the case of Gaussian source is smaller.

B. Model of Thermocapillary Motion

1) Steady-state Migration Velocity: From classical works [1], [3], the thermocapillary migration velocity of a droplet on an open flat container with thin liquid layer is

$$\mathbf{u} = -\frac{2a}{(2 + \frac{\alpha\prime}{\alpha})(2\mu + 3\mu\prime)} \sigma_T \nabla w \tag{14}$$

where μ is the dynamic viscosity of the liquid and α its thermal diffusivity, a is the droplet radius, $\frac{\partial\sigma}{\partial w} = \sigma_T$ the thermal interfacial tension coefficient, w the temperature at droplet position (neglecting the presence of droplet itself). Terms with prime relate to droplet properties, without to liquid properties.

2) Unsteady Thermocapillary Motion: Detailed dynamics can be captured solving Navier-Stokes equations. This problem is widely covered in literature in the approximation of small Reynolds and Marangoni numbers [2]. Actually, estimating Reynolds number with $\rho \approx 1000\,\mathrm{kg/m^3}$, $v \approx 2\,\mathrm{mm/s} \div 5\,\mathrm{mm/s}$, $l \approx 2\,\mathrm{mm} \div 4\,\mathrm{mm}$ and $\mu \approx 0.8\,\mathrm{mPa}$, one gets $Re = \rho v l/\mu \approx 5 \div 25$. Thus, flow can be considered laminar but transient phase is not negligible. Simple models that fit this dynamics with experimental evidence have been found [9].

Lets now apply Newton's approach assuming the droplet to be a point-mass. Considering linear thermocapillary force and quadratic drag force, the droplet equation of motion reads as:

$$\begin{aligned} \dot{\mathbf{x}}_D(t) &= \mathbf{v}_D(t) \\ m\dot{\mathbf{v}}_D(t) &= \mathbf{F}_\sigma(t) + \mathbf{F}_{drag}(t) \\ &= c_1 a^2 \sigma_T \nabla w(t, x_D) - c_2 a^2 \|\mathbf{v}_D(t)\| \mathbf{v}_D(t) \end{aligned} \tag{15}$$

where x_D is droplet position, v_D droplet velocity, m mass, a radius, $\sigma_T = \frac{\partial\sigma}{\partial w}$ liquid-droplet surface tension coefficient, w temperature, c_1 and c_2 scalar parameters. Constant $c_2 = \rho_l C_{drag}/2 > 0$ collects liquid specific mass ρ_l and drag coefficient C_{drag}. All liquid and droplet properties are considered constant with respect to temperature and time.

Constant c_1 may be estimated considering the steady-state condition $\dot{\mathbf{v}}_D = \mathbf{0}$, i.e. when subject to a constant thermal gradient $\widetilde{\nabla w}$ the droplet reaches the steady-state velocity $\mathbf{v}_D^\infty$. In this condition it becomes:

$$\begin{aligned} 0 &= c_1 a^2 \sigma_T \widetilde{\nabla w} - c_2 a^2 \|\mathbf{v}_D^\infty\| \mathbf{v}_D^\infty \\ &\Downarrow \\ c_1 &= \frac{c_2}{\sigma_T} \|\mathbf{v}_D^\infty\| \mathbf{v}_D^\infty \widetilde{\nabla w}^{-1} \end{aligned} \tag{16}$$

Experimentally it was possible to find $\|\mathbf{v}_D^\infty\| \approx 5$ mm/s and then numerically to estimate $\widetilde{\nabla w} \approx -15$ K/m. Other parameters of the experimental setup are reported in Tab. I. Finally, as results from (16), the estimation of thermocapillary force constant is $c_1 \approx 2$.

Lets now consider now the definition of Marangoni number $Ma = -\sigma_T L \Delta w/(\mu\alpha)$—$L$ and Δw characteristic length and temperature difference, μ dynamic viscosity—and try to estimate the surface tension force as $F_\sigma = Ma\mu\alpha = -\sigma_T L \Delta w$. Assuming $\Delta w = -a\nabla w$ and $L = a$ as characteristic quantities, one finds exactly $c_1 = 1$, meaning that the order-of-magnitude of the previous estimation may be correct.

C. Model of Robotic Platform

The robotic platform involved in this project is essentially a 3D printer, with a modular head for syringes, laser and other tools. The kinematics is planar and cartesian and two stepper motors move one axle each. Robot state is described by laser position $\mathbf{x}_L$ and velocity $\dot{\mathbf{x}}_L$ and control inputs are electric signals $\mathbf{I}_L$. Lets consider a generic second-order system to represent the platform, that is:

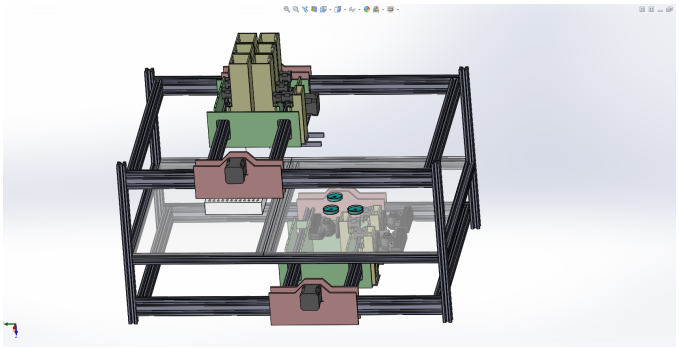

Fig. 4. Robotic platform developed for EVOBLISS project [17]

$$\begin{aligned} \dot{\mathbf{x}}_L &= \mathbf{v}_L \\ M_L(\mathbf{x}_L)\dot{\mathbf{v}}_L &= B_L(\mathbf{x}_L)\mathbf{I}_L - C_L(\mathbf{x}_L, \mathbf{v}_L)\mathbf{v}_L \end{aligned} \tag{17}$$

where it is defined mass matrix M_L, input matrix B_L, damping matrix C_L—not diagonal in general. This model is quite general and comprises many different types of systems. Actually, it reasonably represents stepper motor dynamics under non-slipping conditions. Then, having the platform two independent axles, matrices M_L, B_L and C_L become diagonal. Moreover, the two axes are considered to be equal and independent on the state, so one can replace matrices with three scalar values—m_L, b_L and c_L. Finally, the model reads as:

$$\begin{aligned} \dot{\mathbf{x}}_L &= \mathbf{v}_L \\ m_L\dot{\mathbf{v}}_L &= b_L\mathbf{I}_L - c_L\mathbf{v}_L \end{aligned} \tag{18}$$

III. Optimal Control Problem

A. Formulation

Lets now collect states in vector $\mathbf{z} = [\mathbf{x}_D, \mathbf{v}_D, \mathbf{x}_L, \mathbf{v}_L]^T$ and controls $\mathbf{u} = \mathbf{I}_L$ and define the cost functional J for the time-optimal control problem, with cost on control and laser pointer velocity.

$$\begin{aligned} J &= \int_{t_i}^{t_f} l(t, \mathbf{z}, \mathbf{u}) dt \\ l(t, \mathbf{z}, \mathbf{u}) &= 1 + \frac{w_u}{2}\|\mathbf{u}\|^2 + \frac{w_v}{2}\|\mathbf{v}_L\|^2 \end{aligned} \tag{19}$$

Then, in order to have a fixed final time problem, one applies the linear transformation $t = t_i + (t_f - t_i)\tau$, so that the independent variable becomes $\tau \in [0, 1]$. Doing this, final time t_f becomes a parameter to be optimized and the model

can be written as follows:

$$\begin{aligned}
\frac{d\mathbf{x}_D}{d\tau}(\tau) &= (t_f - t_i)\mathbf{v}_D(\tau) \\
m_D\frac{d\mathbf{v}_D}{d\tau}(\tau) &= (t_f - t_i)\left[b_D\nabla w(\tau, \mathbf{x}_D(\tau)) - c_D\mathbf{v}_D(\tau)\right] \\
\frac{d\mathbf{x}_L}{d\tau}(\tau) &= (t_f - t_i)\mathbf{v}_L(\tau) \\
m_L\frac{d\mathbf{v}_L}{d\tau}(\tau) &= (t_f - t_i)\left[b_L\mathbf{u}(\tau) - c_L\mathbf{v}_L(\tau)\right] \\
w(\tau, \mathbf{x}) &= \bar{w} + \frac{2\beta}{\pi\rho c_p}\sum_j \frac{(t_f - t_i)p_{L,j}\delta\tau}{A_j(\tau)} e^{-\frac{2\|\mathbf{x}-\mathbf{x}_{L,j}\|^2}{A_j(\tau)}} \\
A_j(\tau) &= 8\alpha(\tau - \tau_j)(t_f - t_i) + r_L^2
\end{aligned} \tag{20}$$

subject to initial and final conditions:

$$\begin{aligned}
\mathbf{x}_D(0) &= \mathbf{x}_D^i \qquad & \mathbf{v}_D(0) &= \mathbf{v}_D^i \\
\mathbf{x}_D(1) &= \mathbf{x}_D^f \qquad & \mathbf{v}_D(1) &= \mathbf{v}_D^f \\
\mathbf{x}_L(0) &= \mathbf{x}_L^i \qquad & \mathbf{v}_L(0) &= \mathbf{v}_L^i \\
\mathbf{x}_L(1) &= \mathbf{x}_L^f \qquad & \mathbf{v}_L(1) &= \mathbf{v}_L^f
\end{aligned} \tag{21}$$

In compact form it is:

$$\begin{aligned}
\frac{d\mathbf{z}}{d\tau}(\tau) &= \boldsymbol{\varphi}(\tau, t_f, \mathbf{z}, \mathbf{u}(\tau)) \\
\mathbf{z}(0) &= \mathbf{z}^i \\
\mathbf{z}(1) &= \mathbf{z}^f
\end{aligned} \tag{22}$$

B. Discretisation and Gradient Evaluation

Discretisation of cost function and dynamical constraints makes the optimal control problem a finite dimensional optimisation problem. Building an equispaced time grid, $\tau_k = k\Delta\tau$, and by using explicit forward Euler scheme one can approximate the solution of the ODE that describes the system dynamics, $\mathbf{z}(\tau_k) \approx \mathbf{z}_k$.

$$\begin{aligned}
&\frac{d\mathbf{z}}{d\tau}(\tau) = \boldsymbol{\varphi}(\tau, t_f, \mathbf{z}, \mathbf{u}(\tau)) \\
&\qquad\Downarrow \\
&\frac{\mathbf{z}_{k+1} - \mathbf{z}_k}{\Delta\tau} = \boldsymbol{\varphi}(\tau_k, t_f, \mathbf{z}_0, \ldots, \mathbf{z}_k, \mathbf{u}_k) \\
&\qquad\Downarrow \\
&\mathbf{z}_{k+1} = \mathbf{z}_k + \boldsymbol{\varphi}(\tau_k, t_f, \mathbf{z}_0, \ldots, \mathbf{z}_k, \mathbf{u}_k)\Delta\tau
\end{aligned} \tag{23}$$

Defining the vector of variables $\mathbf{x}$, one can easily express cost function J, equality $\mathbf{g}_{eq}$ and inequality $\mathbf{g}$ constraints in the form requested by *fmincon* function provided by Matlab:

$$\mathbf{x} = [t_f, \mathbf{z}_0, \ldots, \mathbf{z}_N, \mathbf{u}_0, \ldots, \mathbf{u}_N]^T \tag{24}$$

Actually, it is possible to give an analytical expression for the derivatives of these functions, and it is useful to reduce the computational effort:

$$\begin{aligned}
&J[\mathbf{u}] = (t_f - t_i) + \int_{t_i}^{t_f}\left(\frac{w_u}{2}\|\mathbf{u}(t)\|^2 + \frac{w_v}{2}\|\mathbf{v}_L(t)\|^2\right)dt \\
&\qquad\Downarrow \\
&J(\mathbf{x}) = (t_f - t_i)\left[1 + \Delta\tau\sum_{k=0}^{N}\left(\frac{w_u}{2}\mathbf{u}_k^T\mathbf{u}_k + \frac{w_v}{2}\mathbf{v}_{L,k}^T\mathbf{v}_{L,k}\right)\right]
\end{aligned} \tag{25}$$

where $\Delta\tau = 1/N$. Dynamics and boundary conditions are considered as equality constraints:

$$\begin{aligned}
&\mathbf{g}_{eq}(\mathbf{x}) = \\
&= \begin{bmatrix}
\mathbf{z}_0 - \mathbf{z}^i \\
\mathbf{z}_N - \mathbf{z}^f \\
\mathbf{z}_1 - \mathbf{z}_0 - \boldsymbol{\varphi}(\tau_0, t_f, \mathbf{z}_0, \mathbf{u}_0)\Delta\tau \\
\vdots \\
\mathbf{z}_{k+1} - \mathbf{z}_k - \boldsymbol{\varphi}(\tau_k, t_f, \mathbf{z}_0, \ldots, \mathbf{z}_k, \mathbf{u}_k)\Delta\tau \\
\vdots \\
\mathbf{z}_N - \mathbf{z}_{N-1} - \boldsymbol{\varphi}(\tau_{N-1}, t_f, \mathbf{z}_0, \ldots, \mathbf{z}_{N-1}, \mathbf{u}_{N-1})\Delta\tau
\end{bmatrix}
\end{aligned} \tag{26}$$

Finally, cost function derivatives with respect to vector of variables $\frac{\partial J}{\partial \mathbf{x}}$ are:

$$\begin{aligned}
\frac{\partial J}{\partial t_f} &= 1 + \Delta\tau\sum_{k=0}^{N}\left(\frac{w_u}{2}\mathbf{u}_k^T\mathbf{u}_k + \frac{w_v}{2}\mathbf{v}_{L,k}^T\mathbf{v}_{L,k}\right) \\
\frac{\partial J}{\partial \mathbf{u}_j} &= (t_f - t_i)\Delta\tau w_u\mathbf{u}_j^T \\
\frac{\partial J}{\partial \mathbf{z}_j} &= (t_f - t_i)\Delta\tau w_v\mathbf{v}_{L,j}^T
\end{aligned} \tag{27}$$

Derivatives of constraints $\mathbf{g}_{eq}$ have been explicitly derived (not reported here).

C. Model Predictive Control

In this work MPC approach is used to generate a guess solution—i.e. a tentative, suboptimal solution—to initialise the optimisation process. MPC has the ability to anticipate future events—standard PID and LQR have not—and can take control actions accordingly (considering the evolution of a thermal field for instance). Suitable control actions are evaluated in the sense of minimizing a cost function. Thus, the model of the dynamical system is used for calculating step-by-step the optimal next laser spot position (neglecting robot dynamics), taking into account the evolution of the system in a finite time-horizon (MPC is also called *receding horizon control*).

Cost function considered here is the distance between the droplet and a point sliding along the reference trajectory (*sliding control*), computed at the time-horizon (*Mayer term*). In the case of a straight line, the choice of how much to slide is not critical—ensuring that it is large enough to avoid $\Delta x \approx \Delta x_D = v_D\Delta t$. However, this parameter may be time-varying and tuned to affect the high-level behaviour of the controller. For instance, in the case of zero final velocity of the droplet, saturation on the target position allows to estimate a better tentative solution with respect to a constant sliding (that is fine for free final velocity).

At each time step, given the actual state of the system, cost function has to be minimized and to this end *patternsearch* function provided by Matlab is used, because it manages constraints and it is a direct-search algorithm. Notice that cost function derivative with respect to the next laser position may be explicitly derived and used in a gradient-based optimizer, but it is quite involved and this approach is not exploited here.

Then, the calculated time-sequence of laser spot positions is used to reconstruct the control input using inverse dynamics of the robot, Eq. (28). Finally, after checking the feasibility of control input, system evolution is computed again (if needed).

$$\begin{aligned} &\mathbf{x}_{L,k} \qquad k = 1, \ldots, N \\ &\quad \Downarrow \\ &\mathbf{v}_{L,k} = \frac{\mathbf{x}_{L,k+1} - \mathbf{x}_{L,k}}{\Delta t} \\ &\dot{\mathbf{v}}_{L,k} = \frac{\mathbf{x}_{L,k+1} - 2\mathbf{x}_{L,k} + \mathbf{x}_{L,k-1}}{\Delta t^2} \\ &\quad \Downarrow \\ &\mathbf{I}_{L,k} = \frac{m_L}{b_L}\dot{\mathbf{v}}_{L,k} + \frac{c_L}{b_L}\mathbf{v}_{L,k} \end{aligned} \tag{28}$$

The result of this procedure is a feasible guess, i.e. a tentative solution that satisfies constraints—perhaps not final condition $\mathbf{z}(1) = \mathbf{z}^f$.

IV. Simulations

A. Set-up

The approach presented in previous Sections has been tested with two particular final conditions, viz. fixed and free droplet final velocity. Initially both the droplet and the robot are still and the latter is in the origin, final conditions of the robot are free and the reference path is a straight line. The time step used for generating the guess solution with MPC is $\Delta t = 50\,\mathrm{ms}$, but this only defines the refinement of the time grid parametrization. The actual time step depends on the final solution of OCP—on the optimal final time t_f in particular.

Key parameters in the MPC setup are the time horizon $t_h = 1\,\mathrm{s}$ and the sliding $\Delta s = 1$ (given a parametrization of the straight line with $s \in [0, 1]$). Tolerance on mesh size $TolMesh = 10\,\mu\mathrm{m}$ is provided to *patternsearch*, being a trade-off between accuracy and speed in guess solution generation.

In OCP formulation, parameters w_u and w_v define the relative importance of different terms in the cost functional J, Eq. (19). In simulations, unitary values of these weights are considered, i.e. $w_u = 1\,\mathrm{s/A^2}$ and $w_v = 1\,\mathrm{s^3/m^2}$. An *a posteriori* analysis demonstrates that influence of control and velocity cost is small compared to the final time cost, namely

$$N w_v \|\mathbf{v}_L\|^2 \approx N w_u \|\mathbf{u}\|^2 \ll t_f - t_i \tag{29}$$

Other parameters used in simulations are reported in Tab. I.

B. Results and Discussion

Results are here discussed in the case of free and fixed final velocity of the droplet. In particular, results refer to the system evolution obtained considering only the control from the solution of the OCP. This step is done because the optimiser might generate a solution that violates dynamical constraints. Examples of typical laser and droplet trajectories obtained by simulations are shown in Fig. 5 and Fig. 7. It is possible to evaluate all the variables of interest, such as kinematic, dynamic and thermal quantities for instance. See Fig. 6 and Fig. 8 for these variables.

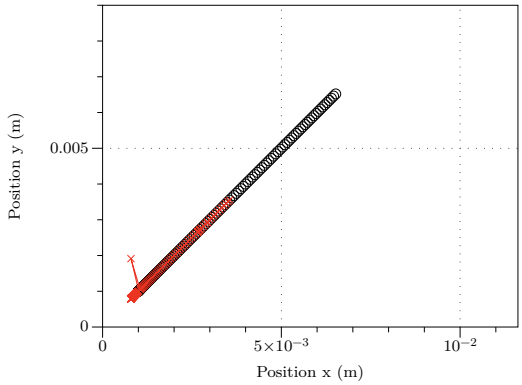

Fig. 5. Droplet and laser trajectories in the case of zero initial and free final velocities (see animation on https://vimeo.com/170754139)

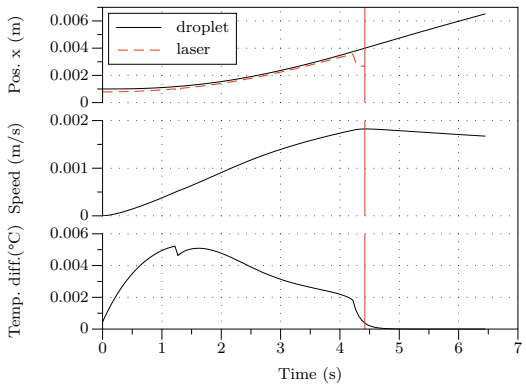

Fig. 6. Temperature, droplet speed, and x positions for laser and droplet in the case of zero initial and final velocities

Let us discuss about the case of free final velocity. It is evident from Fig. 6 that there is an optimal distance between droplet and laser spot. One may analyse this problem considering the case of a continuous laser beam moving at constant speed $\tilde{u}$ along x axis and in quasi-stationary conditions ($\partial w/\partial t = 0$). By defining the spatial coordinate $\xi = x - \tilde{u}t$, the temperature gradient may be expressed as:

$$\nabla w = \nabla w(\xi, \tilde{u}) \tag{30}$$

Then, it can be noticed that in steady-state conditions droplet moves at the same speed $\tilde{u}$ and is subject to a constant thermal gradient $\widetilde{\nabla w} = \nabla w(\tilde{\xi}, \tilde{u})$. So there is a set of possible

TABLE I. Simulation Parameters

Robot	
$p_L = 0.5\,\mathrm{W}$	$r_L = 0.5\,\mathrm{mm}$
$m_L = 1\,\mathrm{kg}$	$b_L = 10\,\mathrm{N/A}$
$c_L = 10\,\mathrm{Ns/m}$	$\lvert i_L \rvert < 1\,\mathrm{A}$
Droplet	
$a = 2\,\mathrm{mm}$	$\rho = 1000\,\mathrm{kg/m^3}$
$\sigma_T = -0.18\,\mathrm{mN/Km}$	$C_{drag} = 0.4$
Liquid	
$\rho = 997\,\mathrm{kg/m^3}$	$c_p = 4186\,\mathrm{J/kgK}$
$k = 0.609\,\mathrm{W/Km}$	$\beta = 0.06\,\mathrm{m^{-1}}$
$\mu = 0.8\,\mathrm{mPas}$	

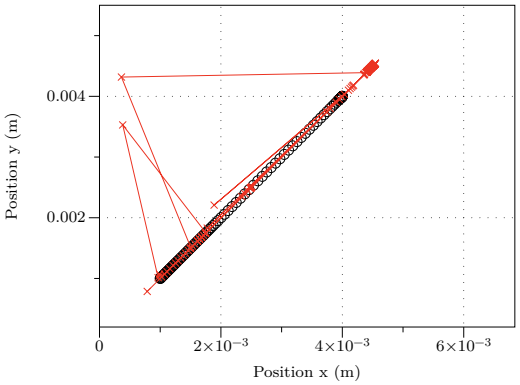

Fig. 7. Droplet and laser trajectories in the case of initial and final velocities both null (see animation on https://vimeo.com/170755486)

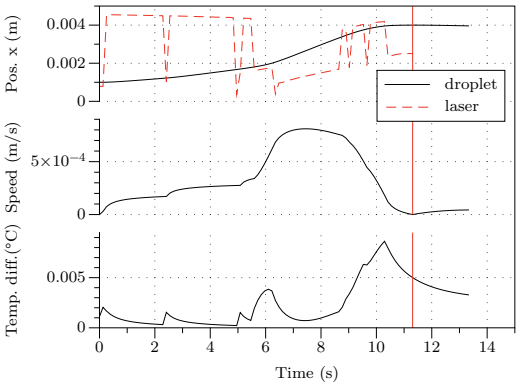

Fig. 8. Temperature, droplet speed, and x positions for laser and droplet in the case of initial and final velocities both null

equilibria $(\tilde{\xi}, \tilde{u})$ defined by the coupling of droplet and thermal dynamics:

$$0 = c_1 \sigma_T \nabla w(\tilde{\xi}, \tilde{u}) - c_2 |\tilde{u}| \tilde{u} \tag{31}$$

Finally, one may formulate an optimisation problem aimed to maximize the steady-state velocity $\tilde{u}$ while satisfying the constraint expressed by Eq. (31). In the case of point source the analytical expression of $\nabla w(\xi, \tilde{u})$ is available, but the aforementioned optimisation problem does not have a simple closed-form solution. However, it is possible to evaluate numerically the optimal pair $(\tilde{\xi}_{max}, \tilde{u}_{max})$ (results omitted here for the sake of brevity).

It is worth to notice that steady state conditions are not reached in the simulated time slot; actually, it seems that the droplet is uniformly accelerated, because speed profile is almost linear. Temperature difference initially arises due to the laser heating, but then decreases as droplet (and robot) speed increases—because less energy per unit volume is released at higher speed. Finally, after stopping the laser heating, droplet is subject to drag and thermocapillary force induced by the residual unsteady temperature field, so without the dominant driving force the droplet slows down.

On the other hand, considering the case of zero final velocity, the optimal strategy is quite different. As reported in Fig. 8, the robot moves repeatedly from behind the droplet to the neighbourhood of the target position. In particular, the robot starts pushing the droplet, it moves close to the target, then it pushes again and finally adjusts the trajectory. So the optimal strategy may be to prepare a thermal gradient needed to stop the droplet while it is just started. It is expected that the timing of these steps would depend on the time constants and the characteristic length of the system. Temperature profile in this case has a maximum close to the final time, because of the initial heating to brake the droplet. Finally, one can notice the lack of symmetry in the laser spot trajectory, Fig. 7. Only few points are captured (due to large robot acceleration and large time step) but it is clear that the laser would shut down in those points, in order to not affect droplet dynamics.

As a final remark, it shall be highlighted the fact that reported results may correspond to local optima found as solution of the OCP.

The model above proposed for the thermal dynamics of the droplet/liquid system has been experimentally validated. In particular, one set of tests has been used for the identification of model parameters, and the resulting, identified model has been then validated by comparison with a different set of tests.

The validation setup is a Petri dish (5 mM, pH 11 decanoate solution, volume 9 ml, 90 mm dish diameter) with a single droplet close to the dish center (lens-shaped droplet, volume 20 µl, 1-decanol). The system temperature was constant and uniform within 0.05°C. An RGB camera has been used for capturing the test area in the Petri dish, using a calibrated image analysis system for measuring absolute and relative positions of droplet and laser beam image. The laser source was a 1.6 W power, 405 nm wavelength unit with a beam diameter of 5 mm.

In the first set of tests, used for calibrating the model parameters, the laser was kept fixed pointing at position close, but not overlapping, to the droplet. The resulting bell-shaped thermal field was pushing the droplet away from the laser spot in radial direction. In the second set of tests, used for validation, the laser was slowly moved against the droplet thus guiding the droplet along a straight path.

Referring to the model in (13)–(15), the physical properties of the liquid medium are known, while the absorption coefficient β, the laser beam radius r_L, the thermocapillary sensitivity c_1, and the friction coefficient c_2 have to be identified. Being the model linear, the effects of β and b_D are undistinguishable from the droplet point-of-view, and only the βb_D product can be identified (see (13) and (15)). In order to take into consideration the actual droplet size (while in the model the droplet is a 1-D point), an additional parameter Δ is introduced to represent the distance between the laser spot and the droplet boundary.

Those parameters have been identified by optimization. In fact, given the system initial conditions, the set of known and guess parameters, and the laser trajectory, it is possible to calculate the evolution of the system according to its analytical model. Then, the actual droplet trajectory and the simulated one can be compared, and the distance between laser spot and droplet center is defined as the optimization metric. The unknown parameters are identified by solving an optimization problem where the target function $\mathcal{J}_{ID}$ is the mean quadratic deviation of the laser-droplet distance between measured and

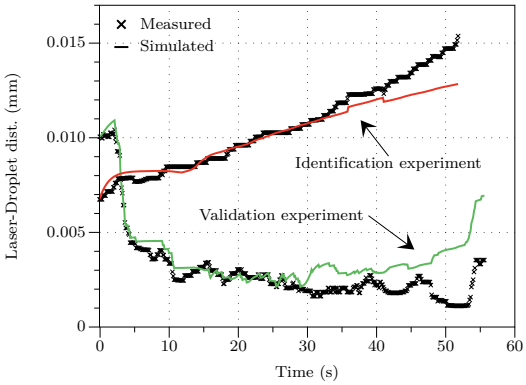

Fig. 9. Comparison of laser-droplet distance evolution for identification and validation experiments, measured and simulated data

simulated experiments, under the constraints of the system dynamics:

$$\mathcal{J}_{ID}(\mathbf{p}) = \sum_{i=0}^{M} \|d(t_{i,m}) - \hat{d}_i\|^2 \tag{32}$$

Once identified, the model has been used in the second set of experiments for forecasting the droplet motion resulting from a given laser spot trajectory (open loop).

The results of the identification and validation steps are reported in Fig. 9. It may be observed as the laser-droplet distance predicted by the model tracks with good approximation (less than the typical droplet diameter) the actual evolution of the system, at least in the first 30 s. After that time, all the experiments (both in identification and validation conditions) show a diverging drift between measured and simulated values. This is probably related to the delayed effect of convective motion of the fluid body, which has not been included in the model. Nevertheless, with the intention of developing a closed loop, model-predictive control of the laser-induced droplet motion this model inadequacy is of limited impact, since in a receding horizon approach the time horizon of 30 seconds is more than enough for implementing a closed loop control.

V. Conclusions and Future Works

This work describes the conceptual framework and the analytical/numerical approach for developing a motion-planning and control system that can be used for driving a droplet in a 2-D liquid field (e.g. a shallow Petri dish), being the motion driver the Marangoni effect.

The approach consists in a two-steps solution of the problem of finding the optimal time-sequence of laser positions that can move the droplet from point A to point B, complying with the dynamics of the droplet dynamics and of the robotic system moving the laser beam, and subjected to constraints on the initial and final condition of the system. The first step is the calculation of a guess solution by application of the *Model Predictive Control* approach. The second step exploits this guess solution for finding a better one by applying the *Optimal Control* theory.

This approach is applied to two different examples, where the droplet is supposed to be moved along a straight line from A to B, where in the first case the droplet velocity in B is unconstrained, while in the second case is constrained to zero. The simulation results show that a rather precise and stable motion control is possible and feasible.

The next step—which is actually an on-going activity—is to use the solution provided by this framework as a control scheme for the robot shown in Fig. 4 thus completing the last dashed box in Fig. 1.

Acknowledgment

M. Hanczyc is financially supported by the European Commission FP7 Future and Emerging Technologies Proactive (EVOBLISS 611640).

References

[1] A. I. Fedosov, "Thermocapillary Motion," *Zhurnal Fizicheskoi Khimii*, vol. 30, no. 2, pp. 366–373, 1956. [Online]. Available: http://arxiv.org/abs/1303.0243

[2] L. H. Dill and R. Balasubramaniam, "Unsteady thermocapillary migration of bubbles," NASA, NASA Technical Report 19890012683, Jan 1988. [Online]. Available: http://ntrs.nasa.gov/search.jsp?R=19890012683

[3] N. Rashidnia and R. Balasubramaniam, "Thermocapillary migration of liquid droplets in a temperature gradient in a density matched system," *Experiments in Fluids*, vol. 11, no. 2–3, pp. 167–174, 1991.

[4] E. Yakhshi-tafti, H. J. Cho, and R. Kumar, "Droplet actuation on a liquid layer due to thermocapillary motion: Shape effect," *Applied Physics Letters*, vol. 96, no. 264101, 2010.

[5] A. Davanlou, R. Shabani, H. J. Cho, and R. Kumar, "Is thermocapillary enough for droplet actuation?" in *17th International Conference on Miniaturized*, no. October. Freiburg, Germany: Systems for Chemistry and Life Sciences, October 2013, pp. 59–61.

[6] A. S. Basu and Y. B. Gianchandani, "Virtual microfluidic traps, filters, channels and pumps using Marangoni flows," *Journal of Micromechanics and Microengineering*, vol. 115031, 2008.

[7] S. Rybalko, N. Magome, and K. Yoshikawa, "Forward and backward laser-guided motion of an oil droplet," *Physical Review E*, vol. 70, no. 046301, pp. 1–4, October 2004.

[8] S.-y. Park and P.-y. Chiou, "Light-Driven Droplet Manipulation Technologies for Lab-on-a-Chip Applications," *Advances in OptoElectronics*, vol. 2011, no. 909174, pp. 1–12, 2011.

[9] D. E. Lucchetta, F. Simoni, L. Nucara, R. Castagna, D. E. Lucchetta, F. Simoni, and L. Nucara, "Controlled-motion of floating macro-objects induced by light Controlled-motion of floating macro-objects induced by light," *AIP Advances*, vol. 077147, no. 2015, 2016. [Online]. Available: http://dx.doi.org/10.1063/1.4927419

[10] M. L. Cordero, D. R. Burnham, C. N. Baroud, and D. McGloin, "Thermocapillary manipulation of droplets using holographic beam shaping: Microfluidic pin ball," *Appl. Phys. Lett.*, vol. 93, no. 034107, 2008.

[11] M. R. de Saint Vincent, R. Wunenburger, and J.-P. Delville, "Laser switching and sorting for high speed digital microfluidics," *Appl. Phys. Lett.*, vol. 92, no. 154105, 2008.

[12] M. M. Hanczyc, "Droplets: Unconventional protocell model with life-like dynamics and room to grow," *Life*, vol. 4, no. 4, pp. 1038–1049, 2014.

[13] M. M. Hanczyc, T. Toyota, T. Ikegami, N. Packard, and T. Sugawara, "Fatty acid chemistry at the oilwater interface: self-propelled oil droplets," *J. Am. Chem. Soc.*, vol. 129, no. 30, pp. 9386–9391, 2007.

[14] J. Čejková, M. Novák, F. Štěpánek, and M. M. Hanczyc, "Dynamics of chemotactic droplets in salt concentration gradients," *Langmuir*, vol. 30, no. 40, pp. 11 937–11 944, 2014.

[15] M. M. Hanczyc, J. M. Parrilla, A. Nicholson, K. Yanev, and K. Stoy, "Creating and maintaining chemical artificial life by robotic symbiosis," *Artif Life*, vol. 21, no. 1, pp. 47–54, 2015.

[16] J. M. P. Gutierrez, T. Hinkley, J. W. Taylor, K. Yanev, and L. Cronin, "Evolution of oil droplets in a chemorobotic platform," *Nature Communications*, vol. 5, no. 5571, 2014.

[17] EVOBLISS 611640 European Commission FP7 Project. [Online]. Available: https://blogit.itu.dk/evoblissproject/

[18] S. L. Anna, "Droplets and bubbles in microfluidic devices," *Annual Review of Fluid Mechanics*, vol. 48, pp. 285–309, 2016.

[19] C. Kunstmann-Olsen, M. Hanczyc, J. Hoyland, S. Rasmussen, and H. Rubahn, "Uniform droplet splitting and detection using lab-on-chip flow cytometry on a microfluidic PDMS device," *Sensors and Actuators B: Chemical*, vol. 229, pp. 7–13, 2016.